Check for updates

Europe
European Chemical
Societies Publishing

▌ **Molecular Recognition**

Enhanced Macroanion Recognition of Superchaotropic Keggin Clusters Achieved by Synergy of Anion–π and Anion–Cation Interactions

Bo Qi,[a] Sai An,[a] Jiancheng Luo,[b] Tianbo Liu,*[b] and Yu-Fei Song*[a]

Abstract: Keggin clusters are the most widely used polyoxometalate building blocks for the construction advanced materials, but effective methods for precisely recognizing the isostructural analogues of Keggins are still limited. In this study we employed the zwitterionic molecule 4,4′-dipyridyl N,N′-dioxide as a recognition receptor to specifically bind to the three Keggin analogues $PW_{12}O_{40}^{3-}$, $PMo_{12}O_{40}^{3-}$, and $SiW_{12}O_{40}^{4-}$, which separately co-assembled into three different types of spherical charged colloids of different sizes. The recognition phenomena were confirmed by electrochemical methods and their crystallization behavior. Compared with solely anion–cation interaction-driven systems, the synergism with the anion–π interactions between the superchaotropic Keggins and the electron-deficient pyridine rings is believed to enhance the recognition. This observation is intriguing as the long-range solution assembly of Keggins is mainly driven by short-range anion–π interactions. Our results show that the little-noticed hydration shell of Keggins is significantly influenced by the superchaotropic effect, leading to differentiated binding affinity to the receptors and more obvious recognition phenomena between tungsten/molybdenum Keggin analogues.

Introduction

Anion recognition in solution has been widely observed in supramolecular chemistry and applied in the fields of sensing, ion extraction, membrane transportation, assembly, and catalysis.[1–5] Macroions, with nanosize and multiple charges, include a large variety of molecular species, ranging from polyhedral oligomeric silsesquioxane (APOSS),[6] borate clusters,[7] polyoxometalates (POMs)[8] to DNA and proteins.[9, 10] An interesting phenomenon of such hydrophilic macroions is that they can recognize each other in dilute solution, by self-assembling into individual assemblies through long-range electrostatic interactions.[11] We have observed this phenomenon in various systems, from the "Keplerate" POM clusters to enantiomeric macroions (chiral recognition).[12, 13] Such molecular clusters are ideal models for understanding biorelevant recognition phenomena.[14] Nevertheless, the solely electrostatic interaction seems to lose its effectiveness for precisely recognizing macroions of smaller size and fewer charges, for example, Keggin
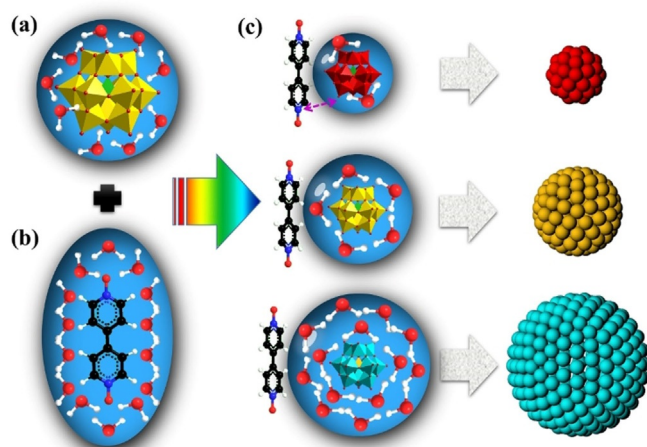
clusters $PW_{12}O_{40}^{3-}$ and $PMo_{12}O_{40}^{3-}$, which implies that some intrinsic properties of Keggin clusters have not been fully revealed.

Keggin macroanions (Scheme 1 a), composed of 12 M–O octahedron shells and an X–O tetrahedral core (M=W, Mo, V; X=P, Si, B, Al, Co, etc.), are among the most popular nanoscale anionic POM clusters with diverse applications in nanoscience, energy conversion, catalysis, and biological systems.[15–19] In recent years, cations or cationic surfactants have often been used to co-assemble with POM anions to construct various superstructures by controlling and directing the interactions. However, for these cationic receptors, effective methods for recognizing POM anions with similar solution behavior are limited, especially in pure water, due to less directional anion–cation interactions.[20–22] Applying electroneutral anion receptors would avoid these disadvantages, for example, by exploiting the superchaotropic effect of POM macroanions recently reported by Stoddart, Bauduin, and Cadot and their co-workers.[23–27] This is exemplified by two very similar Keggins, $PW_{12}O_{40}^{3-}$ and $PMo_{12}O_{40}^{3-}$. They are easily distinguishable from other POMs, such as $SiW_{12}O_{40}^{4-}$, $P_2W_{18}O_{62}^{6-}$, and $P_2W_{17}VO_{62}^{7-}$, by their different superchaotropic behavior, as confirmed by their binding constants with cyclodextrins (CDs),[28] their effect on the cloud point of non-ionic surfactants,[29] or the self-assembly of short-chain poly(N-isopropylacrylamide).[30] However, using these non-ionic receptors to distinguish these tungsten/molybdenum Keggin analogues is still challenging, as relying solely on the chaotropic effect is insufficient. Thus, there is an urgent need for novel macroanion receptors that are capable of forming noncovalent interactions that might exert a synergistic effect in the recognition of these two almost identical

[a] Dr. B. Qi, Dr. S. An, Prof. Y.-F. Song
Beijing Advanced Innovation Center
for Soft Matter Science and Engineering
State Key Laboratory of Chemical Resource Engineering
Beijing University of Chemical Technology, Beijing 100029 (P.R. China)
E-mail: songyf@mail.buct.edu.cn

[b] Dr. J. Luo, Prof. T. Liu
Department of Polymer Science
The University of Akron, Akron, Ohio 44325-3909 (USA)
E-mail: tliu@uakron.edu

📖 Supporting information and the ORCID identification number(s) for the
author(s) of this article can be found under:
https://doi.org/10.1002/chem.202003083.

Chemistry–A European Journal

Full Paper
doi.org/10.1002/chem.202003083

Chemistry
Europe
European Chemical
Societies Publishing

Scheme 1. Illustration of the recognition of Keggin analogues by the dpdo receptor. (a) Structures of Keggin-type POM macroanions: the golden polyhedrons represent the W/Mo-centered oxide octahedrons and the green polyhedron represent the P/Si-O$_4$ tetrahedron. (b) Molecular structure of the zwitterionic recognition receptor 4,4′-dipyridyl N,N′-dioxide (dpdo). C: black, N: blue, O: red, H: white. (c) Recognition of the macroanions PW$_{12}$O$_{40}$$^{3-}$ (red), PMo$_{12}$O$_{40}$$^{3-}$ (yellow), and SiW$_{12}$O$_{40}$$^{4-}$ (cyan) through self-assembly with the dpdo. The purple arrows represent the synergistic effect of the minor anion–cation interaction leading to a smaller globule. Different degrees of dehydration during the binding process lead to separate colloids with different assembly sizes.

Keggin analogues in aqueous solution. In particular, considering the hydration shell, the dimensions of the anions could be affected by their chaotropic effect, so the ability to form short-range interactions, such as anion–π interactions, could be appropriate, because their strength could be significantly influenced by the distance between the anions and the binding site on the receptor.[31–33]

Anion–π interactions, consisting of electrostatic forces and ion-induced polarization, are expected to be prominent players in anion transport, recognition, and catalysis.[34–36] Compared with ion-pair receptors, anion–π receptors have been shown to be more directional to combine with anions. For example, dichloro-substituted tetraoxacalix[2]arene[2]triazine could specifically bind chloride in contrast to the proto analogues.[37] However, inducing long-range self-assembly through short-range anion–π interactions is still a challenging task.[38] Consequently, developing an anion–π-dominated receptor would be helpful for precisely recognizing the Keggin anions, and the molecular structures of the receptors should include the following features. 1) The receptor should have electron-deficient arene rings to offer the desired directional anion–π binding sites to bind the electron-rich Keggin anions. 2) The hydrophobicity should be appropriate,[39] on the one hand, inheriting the advantages of the chaotropic effect of Keggins, which have the propensity to associate with hydrophobic moieties, and on the other hand, preventing entropy-driven self-aggregation, which will block the effective anion–π binding sites. 3) The receptor should have the ability to transform from electron neutral to cationic, thereby introducing the synergism of anion–cation interactions upon recognition. Moreover, there the cationic species should be few to avoid anion–cation inter-
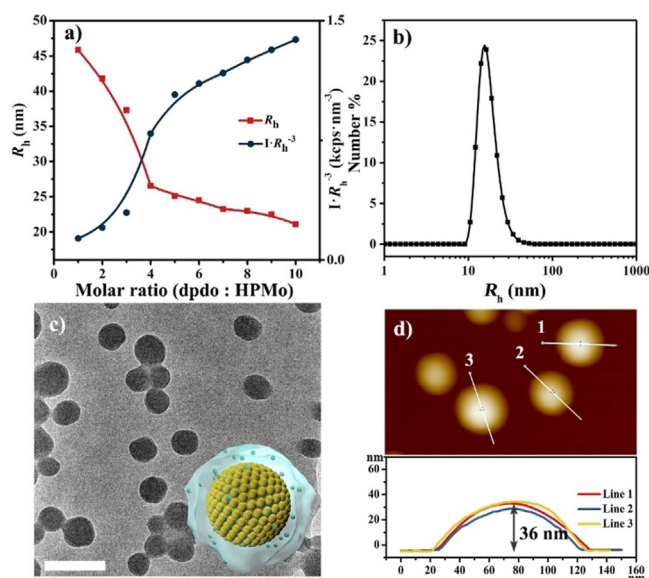
actions competing with the more directional anion–π interactions.

In this study we found that 4,4′-dipyridyl N,N′-dioxide (dpdo), a commonly used ligand in POM crystallography[45] (Scheme 1b), has a surprising and intriguing ability to distinguish precisely the Keggin analogues PW$_{12}$O$_{40}$$^{3-}$, PMo$_{12}O_{40}$$^{3-}$, and SiW$_{12}O_{40}$$^{4-}$. In aqueous solution, the zwitterionic dpdo with electron-deficient pyridine rings can specifically bind to each of these Keggins and co-assemble to form spherical charged colloids with different sizes. The excellent recognition ability of this Keggin receptor was further studied by both electrochemical methods and crystal structure analysis. A recognition mechanism involving the synergy between anion–π interactions, electrostatic interactions, and the superchaotropic effect is proposed based on fluorescence, ^{1}H NMR, and isothermal titration calorimetry (ITC) studies. The strength of the binding interaction was found to be highly sensitive to the thickness of the superchaotropic-affected hydration layer, leading to important recognition phenomena (Scheme 1).

Results and Discussion

Binding ability of dpdo with Keggin H$_3$PMo$_{12}$O$_{40}$ in water

The ability of dpdo to bind to the Keggins and form assembly structures was first measured. Aqueous solutions of both dpdo (ca. 10 mm) and H$_3$PMo$_{12}$O$_{40}$ (HPMo; 1 mm) showed solvent-level intensities in static light scattering (SLS) studies of around 1–10 kcps, which indicates that the Keggin and dpdo exist as single molecules in solutions. After mixing these two solutions, the total scattered intensity of the mixed solution reached a very high scattering intensity of around 8500 kcps, which implies the formation of large structures. The scattering intensity of the mixture became stable after several minutes and their relative size distributions were determined by CONTIN analysis of dynamic light scattering (DLS) data. The results showed that the assemblies formed with a uniform size distribution and without precipitation (Figure 1b). Upon increasing the dpdo concentration from 1 to 10 mm, the average hydrodynamic radii (R_h) of the assemblies decreased and then became almost stable at a dpdo/HPMo molar ratio of more than 4 (Figure 1a, red squares). The concentration of the assemblies (c_A) was determined on the basis of the method reported in the literature.[14] As the intensity $I \propto c_A M_w$, then $c_A \propto I/M_w \propto I/R_h^3$, where M_w is the molecular weight of a single solid spherical assembled particle. This shows that the assembly concentration increases with the addition of more dpdo and that the rate of increment is lower after the addition of more than 4 mm dpdo (Figure 1a, blue spots). Similar R_h values were determined for the assemblies from the DLS data at scattering angles of 90, 75, 60, 45, and 30°, which suggests that the globular structures formed with an average radius of 24.7 nm were spherical. Combined with the radius of gyration (R_g) of 20.9 ± 0.2 nm obtained from the SLS data, the fact that $R_g/R_{h,0} = 0.85 < 1$ suggests that the assemblies were likely solid spheres (see Figure S1 and Table S1 in the Supporting Information). The TEM results further proved the assembly structures were spheres

Chemistry–A European Journal

Full Paper
doi.org/10.1002/chem.202003083

Chemistry
Europe
European Chemical
Societies Publishing

Figure 1. (a) R_h and I/R_h^3 data for aqueous solutions of HPMo (1 mM) and dpdo with the molar ratio of dpdo/HPMo ranging from 1 to 10. (b) CONTIN analysis of the DLS data obtained from a solution composed of dpdo/HPMo = 9:1 (mM) with $R_h \approx 23$ nm. (c) TEM image of globular assemblies with an average diameter of around 45 nm (scale bar = 100 nm). The inset shows a model of the globular assembly in water. (d) Results of the AFM analysis of assemblies with a thickness of 36 nm inferring solid globule structures.

with the radius almost the same as R_h in the solution state (Figure 1 c and Figure S9). Atomic force microscopy (AFM) results indicated that the average height of the assemblies was 36 nm on a solid surface, which suggests the globular assemblies were solid structures (Figure 1 d). Moreover, the zeta potentials of the solutions suggest that the assemblies were negatively charged (see Figure S2). Based on the above observations, a model can be proposed for their formation. The anionic Keggins co-assemble with the dpdo molecules into solid globules and the protons as counter cations are located in the zeta layer of the assemblies and in the bulk water. The Keggin anion lies in the center of the monomer with dpdo and protons randomly distributed around it (Figure 1 c, inset). The self-aggregation of dpdo was ruled out by measuring the conductivities of aqueous dpdo solutions at different concentrations (see Figure S3). A linear relationship was observed between the conductivity and concentration, which indicates a high degree of ionization of dpdo in water and that no aggregates were formed. Moreover, the low scattering intensity of the dpdo solutions observed in the SLS study further support the unassembled state of pure dpdo solutions.

Because dpdo can bind to HPMo to form a heterogeneous new phase, the variation of R_h and c_A with c_{dpdo} suggest that smaller droplets have higher solubility, an interpretation based on the Kelvin equation (Figure 1 a).[40] Here, solutions of 1 mM Keggin in 1 mM dpdo (1dpdo) or 10 mM dpdo (10dpdo) were compared by assuming identical interfacial tension for the same Keggin/dpdo system. In the solution with less dpdo, the dpdo–Keggin attraction was weaker, leading to a lower assembly rate (e.g., $k_{a1} < k_{a10}$). At equilibrium, $k_a = k_d$ (disassembly rate). Thus, we obtain $k_{d1} < k_{d10}$. From the Kelvin equation,

smaller droplets have higher solubility (higher disassembly rate, k_d), therefore the size of the assemblies should follow $R_{h1} > R_{h10}$, which is consistent with experimental results. When c_{dpdo} was over 4 mM, the reaction almost reached equilibrium, which indicates that the binding between dpdo and HPMo is almost saturated.

The binding between dpdo and HPMo was investigated by ^{1}H NMR, fluorescence, and UV/Vis spectroscopy. The oxygen and pyridine nitrogen atoms in dpdo bare negative and positive charges, respectively. Thus, if the oxygen atoms are protonated, anion–cation interactions can form between the Keggin anions and cationic Hdpdo$^+$. The ^{1}H NMR spectra of dpdo show minor changes in the chemical shifts of the α-H in the *ortho* position to the nitrogen atoms after titrating against D$_2$O solutions of HPMo, which suggests that dpdo is less protonated or forms strong hydrogen bonds with HPMo (see Figure S5 in the Supporting Information). Calculations based on the pK_a (0.73 ± 0.15)[44] and the proton concentration (3 × 10^{-3} M) gave a molar ratio of c_{dpdo}/c_{Hdpdo+} of around 64, which means that only a small amount of dpdo is protonated and that most of the molecules are neutral. Thus, the anion–cation attraction between dpdo and Keggins is minor. For the anion–π interactions, the supramolecular crystalline structure of HPMo/dpdo shows directly the binding of PMo^{3-} to the arene rings of dpdo (see Figure 4 b,d). The distances between the rigid ring plane of dpdo and the oxygen atoms in the Keggins are in the range 2.82–2.98 Å, which indicates that the Keggins are indeed captured by the electron-deficient arene rings through anion–π interactions. Further evidence for the anion–π interactions in the solution phase was obtained from the blueshift of the dpdo peaks in the UV/Vis spectra observed upon the addition of HPMo to dpdo solutions, whereas adding the same amount of HClO$_4$ caused no change (see Figure S7). The fluorescence of 10 mM dpdo was quenched by adding acids, including HClO$_4$, HPMo, H$_3$PW$_{12}$O$_{40}$ (HPW), and H$_4$SiW$_{12}$O$_{40}$ (HSiW). However, the quenching effect of the Keggin acids was more significant than that of the "innocent" acid HClO$_4$. In addition, the half widths of the emission peaks of dpdo also changed. Thus, we speculate that these variations may be caused by anion–π interactions (see Figure S8).

Recognition effects on the solution self-assembly of Keggins

After confirming that the dpdo receptor could bind to HPMo to form globular assemblies, the interaction of dpdo with two other very similar Keggins, namely HPW and HSiW, was investigated to see whether the interactions were different. Compared with PMo^{3-}, PW^{3-} exhibits higher polarizability, and SiW^{4-} has a higher charge density. Bauduin and co-workers indicated that HPMo and HPW exhibit similar chaotropic behavior, and that HSiW is less chaotropic.[29] This difference affects their hydration shells and further influences the strength of the anion–π interaction. In addition, HPW is more acidic than HPMo and HSiW, which means the degree of protonation of dpdo is different. These differences would result in a variation in the strength of the binding interaction in the formation of the complexes. Such divergence of driving force leads to differ-

Chemistry–A European Journal

Full Paper
doi.org/10.1002/chem.202003083

Chemistry Europe
European Chemical
Societies Publishing

ent co-assembly phenomena, that is, different recognition in solution.

Specifically, in the complex solutions of the Keggins (1 mм) with dpdo (10 mм), HPW, HPMo, and HSiW show distinct assembly behavior. Considering the two most challenging Keggins for recognition, PW^{3-} and PMo^{3-}, a significant size difference is observed in the TEM images. The average diameter of the HPW assemblies (25 nm) is smaller than that of HPMo (45 nm; Figure 2a,b and Figure S9 in the Supporting Information). This size difference was further confirmed by the DLS results obtained in the solution state (Figure 2d). In the Keggin/ dpdo aqueous solutions, the attraction forces may consist of anion–cation attraction and anion–π interactions. Because the assemblies of PW/dpdo are smaller in size, their radii of curvature are smaller, which results from stronger interfacial tension. Therefore, in accord with the strength of the interfacial tension, the total inner attraction forces in HPW/dpdo globules are stronger. The different strengths of the anion–π interactions can be interpreted as follows: The more chaotropic PW^{3-} with a lower hydration energy can get closer to the arene rings of dpdo, leading to a stronger anion–π interaction. The higher acid strength of HPW results in more protonated dpdo, leading to a stronger anion–cation interaction. Considering that the total attraction forces are mainly composed of anion–π and anion–cation interactions, both of these interactions contribute to the size difference.

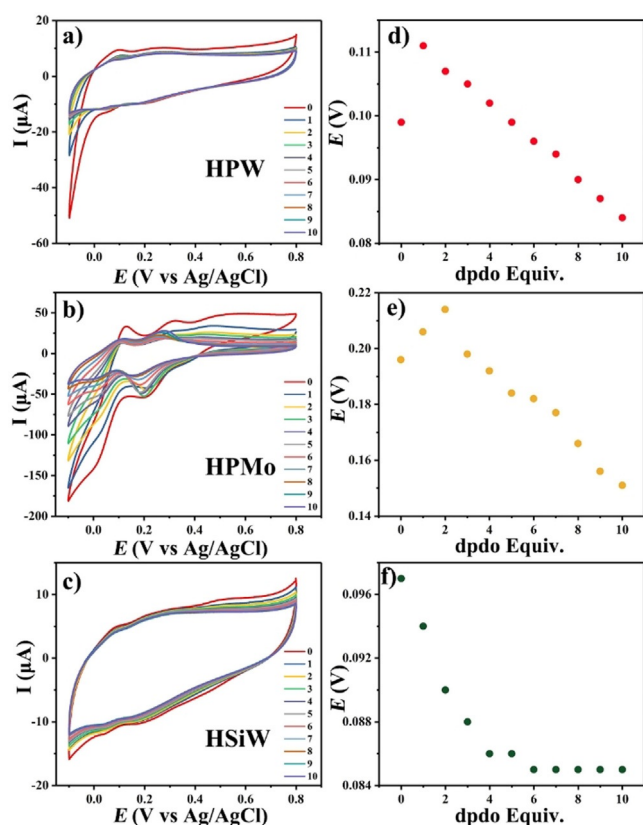For HSiW, globular assemblies were not observed until the concentration of dpdo was over 3 mм, which indicates that HSiW has relatively weak attractions with dpdo. In addition, the absence of assemblies could further obviate the suspicion that the main driving force of self-assembly is the anion–cation attraction. If that is correct, according to Coulomb's law, the anion–cation attraction between $Hdpdo^+$ and SiW^{4-} should be stronger than that between $Hdpdo^+$ and PW^{3-} (or PMo^{3-}). This means that SiW^{4-} should co-assemble with $Hdpdo^+$ more easily and form the smallest globules. However, the average diameter of globules in the system consisting of 1 mм HSiW and 10 mм dpdo is around 120 nm, which is larger than those of both HPW/10dpdo and HPMo/10dpdo (Figure 2c,d). Thus, competitive anion combination in a mixture of HPW/HSiW was investigated. The DLS data (Figure 2e) show that dpdo prefers to bind to HPW to form HPW/dpdo assemblies, and that the amount of assembled HSiW was negligible.

Recognition effects on the electrochemical behavior of Keggins

The influence of dpdo upon the electrochemical properties of the three Keggins was examined. The cyclic voltammogram (CV) of an aqueous solution of 1 mм HPMo exhibited three reversible waves at $+0.364$, $+0.196$, and $+0.012$ V relative to Ag/AgCl (Figure 3b). Upon titration of this solution with dpdo, the second cathodic peak potential first shifted to a higher potential, then continuously decreased to a lower potential, whereas the first cathodic peak remained almost unaltered.
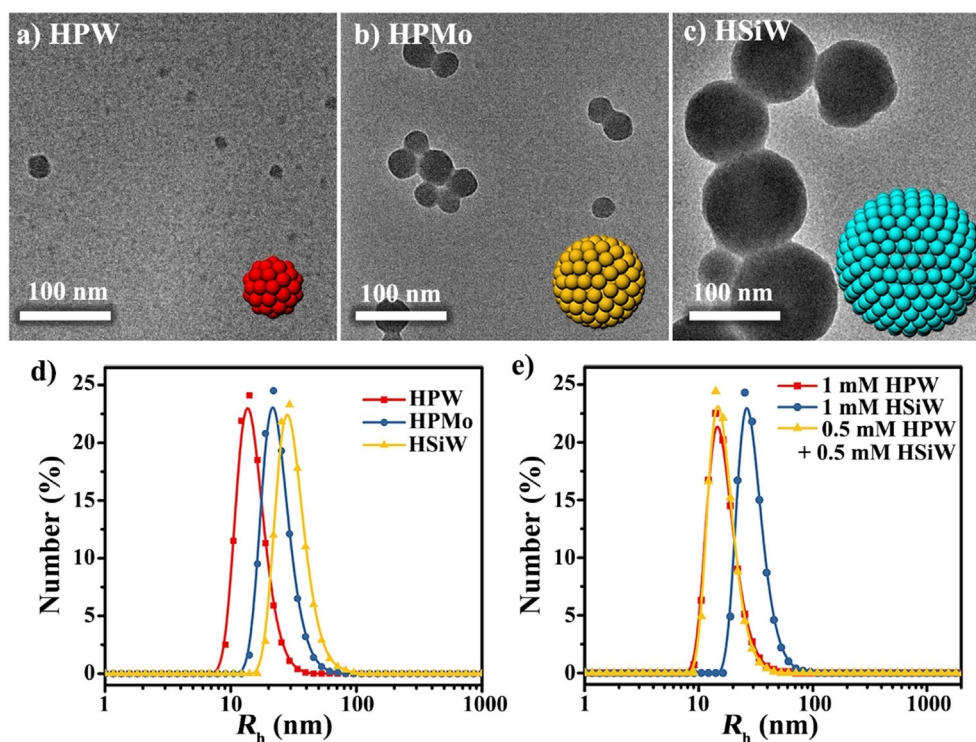
Figure 2. TEM images of the globular mixtures co-assembled from 10 mм dpdo and 1 mм Keggins: (a) HPW, (b) HPMo, and (c) HSiW. The insets represent models of 1-nm-sized Keggin anions self-assembled into globules of different sizes. (d) CONTIN analysis of DLS data from three Keggin/dpdo assemblies showing the same trend in size in aqueous solution. (e) Competitive combination in a solution mixture of dpdo, HPW, and HSiW showing that almost all dpdo assembled with HPW with HSiW remaining as single molecules.

Chemistry–A European Journal

Full Paper
doi.org/10.1002/chem.202003083

Chemistry Europe
European Chemical
Societies Publishing

Figure 3. Cyclic voltammograms (298 K, scan rate 100 mV s^{-1}) of 1 mM aqueous solutions of b HPW, (b) HPMo, and (c) HSiW Keggins in the presence of increasing amounts of dpdo from 1 to 10 mM. (d–f) Plots of the peaks with the most significant change in potential (first anodic peak potential of HPW (d) and HSiW (f) and second cathodic peak potential of HPMo (e)) versus the equivalent number of dpdo, showing a two-step sequential binding process.
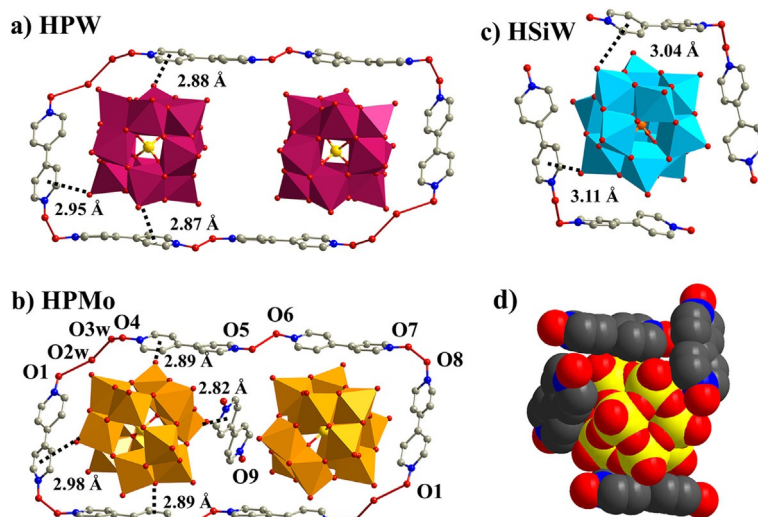
The peak shift is mainly attributed to a variation in the environment around the Keggin clusters.

A large number of hydration water molecules around the Keggins are replaced by a small amount of organic dpdo. Thus, the stability of the reduced form of the Keggins may correspondingly change.[41] Remarkably, the addition of dpdo caused only an indistinct change in the CVs of HPW and HSiW (Figure 3 a,c), in contrast to the behavior of HPMo. This suggests that the zwitterionic dpdo can discriminately affect the redox properties of Keggin macroanions in water. The plots of the change in peak potential versus dpdo equivalents in Figure 3 d–f clearly show a transition point in all three Keggin CV curves, inferring a two-step sequential binding process. Moreover, the transition points in the stoichiometric conditions are quite similar to the binding number (n) of dpdo/POM interactions obtained from the ITC experiments (see Table 1), which reflects the efficiency of the breaking of the hydration shells of the Keggin macroanions.

Recognition effects on the crystallization behavior of Keggins

Because the HPMo/dpdo system shows distinctive assembly behavior compared with the other Keggins, single crystals of

H$_3${dpdo$_{3.5}$PMo$_{12}$O$_{40}$} suitable for X-ray diffraction analysis were obtained to clarify the interactions between dpdo and HPMo (Figure 4 b). Structural analysis revealed that the crystal unit cell consists of two PMo^{3-} anions and seven dpdo ligands, with the protons located on the oxygen atoms of dpdo or water molecules. The PMo^{3-} anions are surrounded by the seven dpdo ligands, one of which is centered between the two Keggin molecules and the other six dpdo molecules are linked through hydrogen bonding with water to form a rectangular belt. Single crystals of H$_3${dpdo$_3$PW$_{12}$O$_{40}$} and H$_4${dpdo$_4$SiW$_{12}$O$_{40}$} were also analyzed to clarify the influence of the dpdo on the crystallization behavior of the Keggins (Figure 4 a,c). The binding numbers of dpdo with HPW, HPMo, and HSiW are 2:6, 2:7, and 2:8, respectively. This trend reflects the trend of the transition points observed in the CV experiments. The unit cell of HPW/dpdo shows a similar structure to HPMo/dpdo, but without the dpdo molecule located in the core of the unit cell between the Keggins. The locations of the protons were determined on the basis of the O···O distances. The corresponding O–H···O bonds can be classified into three types: 1) Hydrogen bonds between water molecules (d(O2w···O3w) = 2.65(4) Å, d(O3w···O3w′) = 2.53(2) Å), 2) hydrogen bonds between dpdo molecules (d(O5···O6) = 2.57(2) Å, d(O7···O8) = 2.66(2) Å), and 3) hydrogen bonds between dpdo and water (d(O2w···O1) = 2.72(4) Å, d(O2w···O8′) = 2.36(4) Å, d(O3w···O4) = 2.49(1) Å). These short O···O distances indicate that the dpdo molecules could combine with water molecules through very strong hydrogen bonding; according to Gilli and co-workers,[43] very short hydrogen bonds (O···O = 2.2–2.5 Å) belong to negative-charge-assisted hydrogen bonds, that is, O–H···O$^-$, which transform from a dissymmetrical electrostatic interaction to an interaction with increasingly covalent character. Thus, the O4 and O8 atoms are not protonated in this structure and O1 is neutralized by a proton, resulting in a relatively long hydrogen bond. Furthermore, in such a crystallization, the W–O bond distances and W–O–W angles are all similar to those of typical Keggin PMo^{3-} structures, which rules out the possibility that the protons are located on the surfaces of the POM anions. In HSiW/dpdo, the SiW^{4-} anion is surrounded by four protonated dpdo ligands. However, complex hydrogen-bonding networks are not observed in the HSiW/dpdo structure (see Figure S13 and Table S2 in the Supporting Information). The dpdo molecules form zig-zag 1D chains along the c axis, and these chains are hexagonally stacked along the ab plane (see Figure S12). From the perspective of the stacking model, HSiW/dpdo forms a 1D chain, whereas the others form 3D supramolecular frameworks (see Figure S11). Thus, HSiW/dpdo crystallizes in the monoclinic space group $C2/C$, whereas HPW/dpdo and HPMo/dpdo crystallize in the triclinic space group $P\bar{1}$. Moreover, the distances from the centroids of the pyridine rings to the nearest oxygen atoms of the Keggins were measured. A relatively long distance was determined in HSiW/dpdo compared with in HPW/dpdo and HPMo/dpdo, which indicates that the anion–π interactions in HPW/dpdo and HPMo/dpdo are stronger than those in HSiW/dpdo.

Chemistry–A European Journal

Full Paper
doi.org/10.1002/chem.202003083

Chemistry Europe
European Chemical
Societies Publishing

Figure 4. Representations of the supramolecular structures (a) HPW/dpdo, (b) HPMo/dpdo, and (c) HSiW/dpdo determined by X-ray diffraction analysis showing the different binding numbers between dpdo and the Keggin POM macroanions. The dashed lines represent the anion–π interactions between the POM anions and pyridine rings of dpdo. (d) Space-filling model of HPMo/3.5dpdo supramolecular structure reveals the binding mode between Keggin anions and the dpdo receptor.

Recognition mechanism and the binding process

The distinct recognition phenomena of the Keggins HPW and HPMo shed light on the recognition mechanism for the Keggins. Interestingly, no assemblies were observed by changing the counter ions of PMo_{12}^{3-} from H^+ to Na^+, and globules of HPMo/dpdo of similar size and morphology appeared after introducing a certain amount of HCl into solution (Figure 5). This indicates that the protons play a crucial role in the recognition process and that the acidic strength of the Keggins may have a synergistic effect on the binding affinity by affecting the minor anion–cation interactions.
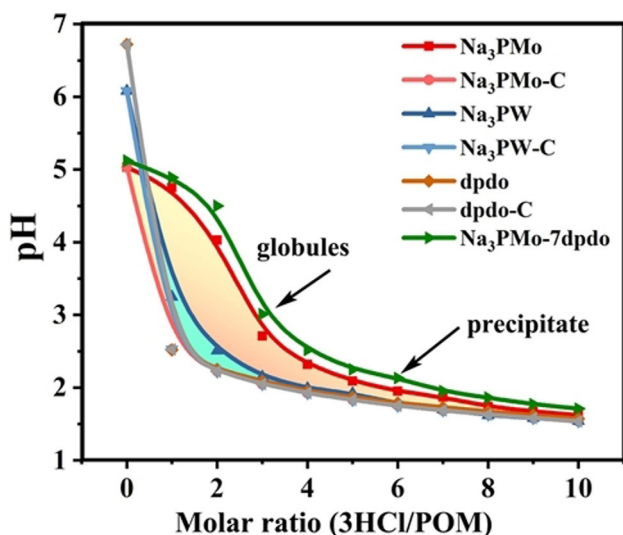
Figure 5. pH variation of aqueous solutions of $Na_3PMo_{12}O_{40}$ (Na_3PMo), $Na_3PW_{12}O_{40}$ (Na_3PW), dpdo, and $Na_3PMo_{12}O_{40}/7dpdo$ upon addition of 3HCl, together with the respective calculated curves Na_3PMo-C, Na_3PW-C, and dpdo-C showing the pH variation upon adding 3HCl to blank water with same initial pH value.

To probe the binding model of the protons, solutions of Na_3PMo (red line) and dpdo (brown line) were separately titrated against HCl (Figure 5). Two calculated curves (Na_3PMo-C and dpdo-C) are also included in Figure 5 to show the variation in pH values when HCl was added to blank water with the same initial proton concentration. If the titration curve is the same as that of the corresponding calculated curve, then the protons in solution have only a minor binding affinity for the solutes. Figure 5 shows that the dpdo curve overlaps with the calculated curve (dpdo-C), which indicates that the proton affinity of dpdo is lower than that of the PMo anions.

^{1}H NMR studies revealed the protonation state of dpdo in more detail. By continuously adding HCl to the dpdo solution, a clear shift in the signal was observed, which suggests an increase in the degree of protonation of dpdo, that is, the number of $Hdpdo^+$ increased. By contrast, adding 1 mM Keggins caused an inconspicuous chemical shift, which indicates that most of the dpdo molecules are charge-neutral. Superimposition of the ^{1}H NMR spectra of the three Keggin/dpdo complexes showed that the peak shift of HP(Si)W/dpdo was slightly larger than that of HPMo/dpdo, representing a higher degree of protonation of dpdo (see Figures S4 and S6 in the Supporting Information). Unlike the almost complete overlap of the dpdo curves (dpdo and dpdo-C) in Figure 5, the curves of Na_3PMo and Na_3PMo-C form a loop, which indicates the association of PMo^{3-} with added protons. The narrower loop of the curves formed by Na_3PW and Na_3PW-C indicates that the PW^{3-} anions have a lower affinity for protons. The differences in proton affinity can be understood in terms of their acid strengths (HPW > HSiW > HPMo).[42] The higher acid strength of HPW means that more dpdo molecules are protonated, and the larger number of $Hdpdo^+$ leads to stronger anion–cation attractions than is the case for HPMo. Thus, the assemblies of HPW/dpdo are significantly smaller than those of HPMo/dpdo,

Chemistry–A European Journal

Full Paper
doi.org/10.1002/chem.202003083

Chemistry Europe
European Chemical
Societies Publishing

combining with the synergism of superchaotropic-affected anion–π interactions.

Based on the above analysis, the state of the protons can be clarified. The fully dissociated protons transfer to three states after the addition of dpdo to pure Keggin solutions. First, a small number of protons combine with the oxygen in dpdo to allow anion–cation interactions to form between the Keggin anions and Hdpdo$^+$. The degree of protonation is related to the acid strength of the Keggins. Direct evidence for the protonation of dpdo can also be obtained from the fluorescence spectra: The fluorescence of dpdo is significantly quenched due to the formation of hydrogen bonds between Hdpdo$^+$ and solvation water molecules, resulting in the transfer of an excited-state proton to quench the fluorescence (see Figure S8a in the Supporting Information). Secondly, a large number of protons remain in the bulk water, which is supported by the negative zeta potential of the colloids. Thirdly, the remaining protons are incorporated into the colloids and form ion-pair bonds with the Keggin anions. In comparison with PW^{3-}, the higher proton affinity of PMo^{3-} leads to a large decrease in intermolecular electrostatic repulsion, which results in larger assembly sizes.

ITC experiments were performed to further elucidate the recognition mechanism of the Keggin/dpdo self-assembly process and determine the binding strengths of the complexes formed. HPMo, HPW, and HSiW solutions (200 μL, 1 mм) were each titrated against a solution of dpdo (40 μL, 40 mм) at 288 K (Figure 6). These three experiments showed similar exothermic binding processes. As further dpdo was injected, the heat produced first increased and then gradually decreased after a certain transition point, finally reaching an almost saturated situation. The two different phases in the ITC curves indicate that two binding processes co-exist and that the binding sites are not identical. Because of the hydration shells around both the Keggin anions and dpdo zwitterions, the association of the two species is associated with the breakage of the hydration shells, and the structural water molecules are released from the hydration shells into the bulk water phase.

For the superchaotropic Keggins, the hydration shell breakage is exothermic. For the arene rings of dpdo, the breakage of the hydration shell is endothermic.[39] Thus, the first binding process includes breakage of the hydration shells and the combination of the two species to form anion–π interactions. The rate of heat release from the combination process is greater than the heat absorption rate of the breakage process. When the concentration of dpdo reaches the transition point, the breakage of the hydration shell is almost saturated. From the ITC curves of the different Keggins, the molar ratio values at the transition point increase in the sequence HPW < HPMo < HSiW, which is consistent with the sequence of their superchaotropic effect. The SiW^{4-} anion with the weakest superchaotropic effect has the strongest anion hydration, thus leading to the least efficient dehydration during the combination process due to the release of the smallest number of water molecules. The highest hydration energy results in the thickest hydration shell around SiW^{4-}, which prevents the Keggins approaching the arene rings, so the anion–π interactions between SiW^{4-} and dpdo are the weakest, which means that the HSiW/2dpdo solutions, despite their stronger electrostatic attraction, cannot assemble into globules, unlike HPW(Mo)/2dpdo.

In addition, the thermodynamic parameters of the interactions between dpdo and the three Keggins can be obtained by fitting these ITC curves (Figure 6 and Table 1). The results of the ITC analysis show a quite significant affinity between HPMo and dpdo, with $K_{a1} = 1.08 \times 10^4 \, \text{м}^{-1}$ and $K_{a2} = 2.53 \times 10^3 \, \text{м}^{-1}$. These binding constants are comparable to those reported by Stoddart and co-workers for the host–guest complexes of γ-CD and the Keggins.[27] For the purpose of simplifying the fitting procedure and focusing on the combination process between dpdo and the Keggins, the second part of the titration curve was fitted by an independent model to rep-
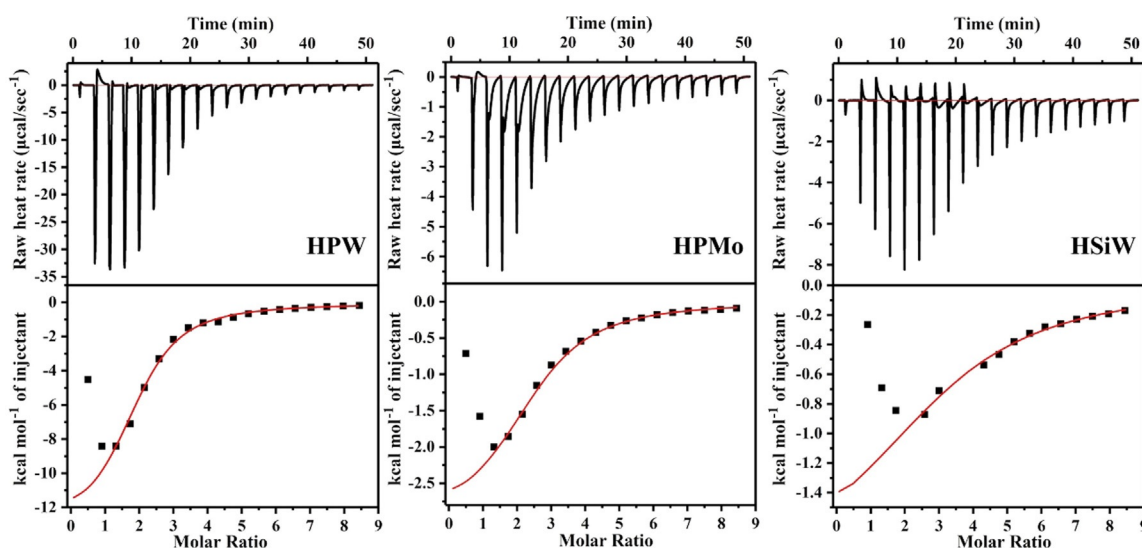
Figure 6. Results of ITC experiments performed at 288 K by sequential injection of 40 μL of 40 mм dpdo solution into 200 μL of 1 mм HPW, HPMo, or HSiW solutions (top). Fitting of the second phase of the titration curve by the independent model (bottom).

Chemistry–A European Journal

Full Paper
doi.org/10.1002/chem.202003083

Chemistry Europe
European Chemical
Societies Publishing

Table 1. ITC results for the titration of dpdo into different POM solutions.

	HPW	HPMo	HSiW
K_a [M^{-1}]	3600	2230	724
n	1.9	2.4	3.3
ΔH [kcal mol^{-1}]	−13.26	−3.05	−1.98
$T\Delta S$ [kcal mol^{-1}]	−8.56	1.34	1.79

resent the thermodynamic parameters of the pure combination process (Figure 6, bottom, and Table 1). The fitting data of the second part of HPMo curve by the independent model is similar to the data obtained by fitting the whole curve with two-step sequential binding modes (see Figure S14 in the Supporting Information). The results indicate that HPW has the greatest affinity for dpdo in aqueous solution. The strongest binding of HPW/dpdo can be attributed to the synergism of the predominant anion–π interaction and the minor anion–cation attraction: 1) The most effective dehydration of the superchaotropic PW^{3-} results in the shortest anion–arene distance, leading to the strongest anion–π binding and 2) the stronger acid strength of HPW results in more dpdo being protonated, that is, a stronger electrostatic attraction. The cooperation of these influences produces the smallest HPW/dpdo globules (Scheme 1).

The variation in the binding numbers for dpdo and the Keggins is consistent with the results of the CV experiments and single-crystal structure analysis. The thermodynamic parameters suggest that the binding between the Keggins and dpdo is mainly driven by an enthalpic process. The results show that the entropy change in the HPW system is negative, and positive in the other systems. This behavior can be explained by the entropy decrease invoked by the dehydration of the less ordered Keggin hydration water and recovery of more ordered bulk water molecules and the entropy increase incurred by the dehydration of the highly ordered water molecules around the arene rings of dpdo, respectively. For HPW/dpdo, fewer dpdo combine and the dehydration of PW^{3-} is more dominant, leading to the negative change in the entropy. For HPMo and HSiW, more dpdo molecules would combine as the less chaotropic Keggins undergo less efficient dehydration, thus the dehydration of water molecules around arene rings becomes more dominant resulting in the positive entropy changes.

Conclusion

We have demonstrated here that the Keggin macroanions, especially PW$_{12}$O$_{40}$$^{3-}$ and PMo$_{12}$O$_{40}$$^{3-}$, can be well recognized through their assembly with the zwitterionic dpdo receptor. The combination of Keggins and dpdo in aqueous solution leads to the formation of globules with controllable sizes. The self-assembly of the different Keggin anions with dpdo shows remarkably distinct features, such as different sizes of globular assemblies, as well as different electrochemical properties and co-crystallization behavior. The study of the recognition mechanism revealed that the assembly is driven by the synergism of the anion–π interaction and electrostatic attraction, that the di-

rectional anion–π interaction is predominant and the contribution of the less directional anion–cation attraction is minor. In detail, the stronger chaotropic Keggins result in more effective dehydration, leading to stronger anion–π interactions, whereas more acidic Keggins result in more protonated dpdo, which results in a stronger anion–cation interaction. It should be noted that the synergistic effect of the minor anion–cation attraction is a unique advantage of zwitterionic receptors that neutral non-ionic receptors do not have. This study highlights a promising approach to recognizing macroanions, such as boron clusters, proteins, and DNA fragments, in aqueous solutions in a more general way.

Experimental Section

Solution studies: The aqueous solutions of the complexes were prepared by direct mixing of mother aqueous solutions of dpdo and the Keggins with higher concentration. The aqueous solutions of the complexes were stored for various times for further characterization. The morphologies of the assemblies were investigated by scanning electron microscopy (SEM Zeiss Supra 55) and transmission electron microscopy (TEM Hitachi H800). The surface roughness and thickness data were obtained by AFM and analyzed by using the Nanoscope analysis software. The ^{1}H NMR spectra were recorded on a Bruker AV400 NMR spectrometer at a resonance frequency of 400 MHz, and the chemical shifts reported relative to H$_2$O as the internal reference.

Zeta-potential and particle size analyses were performed with a Malvern Mastersize 2000 zeta and size analyzer, respectively. The intensities of the solutions and size distributions of different testing angles were measured by using a commercial Brookhaven Instrument LLS spectrometer equipped with a solid-state laser operating at 532 nm. SLS experiments were performed at scattering angles (θ) between 30 and 120°, at intervals of 2°. A partial Zimm plot derived from the Rayleigh–Gans–Debye equation was used to analyze the SLS data to obtain the radii of gyration (R_g). The partial Zimm plot stems from the following approximate formula: $1/I = C(1+R_g^2(q^2/3))$, and R_g can be determined from the slope and the intercept of a plot of $1/I$ versus q^2. DLS analysis was performed by using a BI-200SM multichannel digital correlator to measure the intensity–intensity time correlation function. From the DLS measurements, the particle size distribution in solution was obtained from a plot of the intensity versus R_h.

Electrochemistry: CV experiments were carried out at room temperature in H$_2$O with a CHI660E electrochemical workstation. All CV experiments were performed by using a platinum working electrode. The electrode surface was polished routinely with a 0.05 μm alumina/water slurry on a felt surface immediately before use. An S3 Pt coil was used as the counter electrode and Ag/AgCl electrode as the reference electrode. Keggin solutions were prepared at a concentration of 1 mM, and 100 mM dpdo solutions were titrated into the Keggin solutions with different molar ratios.

Keggin/dpdo single crystals: Single crystals of Keggin/dpdo complexes were obtained by the layer-by-layer diffusing method. The bottom layer of the dpdo aqueous solution (22 mg, 0.10 mmol) was first injected into the mixing tube, and then a diffusing layer consisting of a solution (6 mL) of acetonitrile/water (3:2, v/v) was carefully layered upon the bottom layer, and finally a solution of the Keggin in acetonitrile/water (6:2, v/v; 4 mL) was carefully added as the top layer. Plate crystals appeared after 4–5 weeks. These were collected and washed with EtOH. The crystals of HPW/

dpdo, HPMo/dpdo, and HSiW/dpdo are orange, yellow, and colorless, respectively.

Single-crystal XRD analyses: Single-crystal X-ray data were measured at 153 K on a Rigaku SuperNova Atlas S2 diffractometer (Cu$_{K\alpha}$, $\lambda = 1.54178$ Å) equipped with a graphite monochromator. Data collection and structure refinement details can be found in the in the Supporting Information, including the CIF files.

Deposition numbers 1974126 (HPW/dpdo), 1948875 (HPMo/dpdo), and 1984274 (HSiW/dpdo) contain the supplementary crystallographic data for this paper. These data are provided free of charge by the joint Cambridge Crystallographic Data Centre and Fachinformationszentrum Karlsruhe Access Structures service.

Isothermal titration calorimetry: All ITC experiments were performed in an isothermal calorimeter (ITC$_{200}$, MicroCal, USA). First, 1 mm solutions of different Keggins were placed in a 200 µL calorimetric cell. Then, 40 mm dpdo was used to titrate the sample solution. The Keggin solutions were injected into the calorimetric cell with a clean syringe, and the dpdo solution was loaded into a 40 µL calorimetry syringe. The temperature of the cell was set at 15 °C. The injection volume was set at 2 µL each time within 4 s. A delay of 150 s was applied between each injection. The solutions were mixed at 1000 rpm. The heat of dilution for each addition of dpdo (background heat) was determined by using the same concentration of dpdo that was used for the Keggin solutions, only with water (200 µL) in the cell instead of the Keggin solution.

Conflict of interest

The authors declare no conflict of interest.

[1] M. J. Langton, C. J. Serpell, P. D. Beer, *Angew. Chem. Int. Ed.* **2016**, *55*, 1974–1987; *Angew. Chem.* **2016**, *128*, 2012–2026.
[2] D. Zhang, T. K. Ronson, J. Mosquera, A. Martinez, J. R. Nitschke, *Angew. Chem. Int. Ed.* **2018**, *57*, 3717–3721; *Angew. Chem.* **2018**, *130*, 3779–3783.
[3] N. Busschaert, C. Caltagirone, W. Van Rossom, P. A. Gale, *Chem. Rev.* **2015**, *115*, 8038–8155.
[4] P. A. Gale, E. N. W. Howe, X. Wu, *Chem.* **2016**, *1*, 351–422.
[5] A. J. Neel, M. J. Hilton, M. S. Sigman, F. D. Toste, *Nature* **2017**, *543*, 637–646.
[6] W. Zhang, X. Dong, S. Z. D. Cheng, *Chem.* **2019**, *5*, 492–493.
[7] K. I. Assaf, M. S. Ural, F. Pan, T. Georgiev, S. Simova, K. Rissanen, D. Gabel, W. M. Nau, *Angew. Chem. Int. Ed.* **2015**, *54*, 6852–6856; *Angew. Chem.* **2015**, *127*, 6956–6960.
[8] X.-S. Hou, G.-L. Zhu, L.-J. Ren, Z.-H. Huang, R.-B. Zhang, G. Ungar, L.-T. Yan, W. Wang, *J. Am. Chem. Soc.* **2018**, *140*, 1805–1811.
[9] N. H. Evans, P. D. Beer, *Angew. Chem. Int. Ed.* **2014**, *53*, 11716–11754; *Angew. Chem.* **2014**, *126*, 11908–11948.
[10] R. Chakraborty, K. K. Kidd, *Science* **1991**, *254*, 1735–1739.
[11] P. Yin, J. Zhang, T. Li, X. Zuo, J. Hao, A. M. Warner, S. Chattopadhyay, T. Shibata, Y. Wei, T. Liu, *J. Am. Chem. Soc.* **2013**, *135*, 4529–4536.
[12] T. Liu, M. L. K. Langston, D. Li, J. M. Pigga, C. Pichon, A. M. Todea, A. Müller, *Science* **2011**, *331*, 1590.
[13] P. Yin, Z.-M. Zhang, H. Lv, T. Li, F. Haso, L. Hu, B. Zhang, J. Bacsa, Y. Wei, Y. Gao, Y. Hou, Y.-G. Li, C. L. Hill, E.-B. Wang, T. Liu, *Nat. Commun.* **2015**, *6*, 6475.
[14] J. Zhang, D. Li, G. Liu, K. J. Glover, T. Liu, *J. Am. Chem. Soc.* **2009**, *131*, 15152–15159.
[15] L. Cronin, A. Müller, *Chem. Soc. Rev.* **2012**, *41*, 7333–7334.
[16] C. L. Hill, *Chem. Rev.* **1998**, *98*, 1–2.
[17] D.-Y. Du, L.-K. Yan, Z.-M. Su, S.-L. Li, Y.-Q. Lan, E.-B. Wang, *Coord. Chem. Rev.* **2013**, *257*, 702–717.
[18] J. J. Berzelius, *Ann. Phys.* **1826**, *82*, 369–392.
[19] J. F. Keggin, *Nature* **1933**, *131*, 908–909.
[20] B. Li, W. Li, H. Li, L. Wu, *Acc. Chem. Res.* **2017**, *50*, 1391–1399.
[21] A. Misra, K. Kozma, C. Streb, M. Nyman, *Angew. Chem. Int. Ed.* **2020**, *59*, 596–612; *Angew. Chem.* **2020**, *132*, 606–623.
[22] A. Nisar, X. Wang, *Dalton Trans.* **2012**, *41*, 9832–9845.
[23] T. Buchecker, X. Le Goff, B. Naskar, A. Pfitzner, O. Diat, P. Bauduin, *Chem. Eur. J.* **2017**, *23*, 8434–8442.
[24] C. Falaise, M. A. Moussawi, S. Floquet, P. A. Abramov, M. N. Sokolov, H. Haouas, E. Cadot, *J. Am. Chem. Soc.* **2018**, *140*, 11198–11201.
[25] M. A. Moussawi, M. Haouas, S. Floquet, W. E. Shepard, P. A. Abramov, M. N. Sokolov, V. P. Fedin, S. Cordier, A. Ponchel, E. Monflier, J. Marrot, E. Cadot, *J. Am. Chem. Soc.* **2017**, *139*, 14376–14379.
[26] B. Naskar, O. Diat, V. Nardello-Rataj, P. Bauduin, *J. Phys. Chem. C* **2015**, *119*, 20985–20992.
[27] Y. Wu, R. Shi, Y.-L. Wu, J. M. Holcroft, Z. Liu, M. Frasconi, M. R. Wasielewski, H. Li, J. F. Stoddart, *J. Am. Chem. Soc.* **2015**, *137*, 4111–4118.
[28] M. A. Moussawi, N. Leclerc-Laronze, S. Floquet, P. A. Abramov, M. N. Sokolov, S. Cordier, A. Ponchel, E. Monflier, H. Bricout, D. Landy, M. Haouas, J. Marrot, E. Cadot, *J. Am. Chem. Soc.* **2017**, *139*, 12793–12803.
[29] T. Buchecker, P. Schmid, S. Renaudineau, O. Diat, A. Proust, A. Pfitzner, P. Bauduin, *Chem. Commun.* **2018**, *54*, 1833–1836.
[30] T. Buchecker, P. Schmid, I. Grillo, S. Prévost, M. Drechsler, O. Diat, A. Pfitzner, P. Bauduin, *J. Am. Chem. Soc.* **2019**, *141*, 6890–6899.
[31] Y. Marcus, *Chem. Rev.* **1988**, *88*, 1475–1498.
[32] Y. Marcus, *Chem. Rev.* **2009**, *109*, 1346–1370.
[33] B. Qi, X. Guo, Y. Gao, D. Li, J. Luo, H. Li, S. A. Eghtesadi, C. He, C. Duan, T. Liu, *J. Am. Chem. Soc.* **2017**, *139*, 12020–12026.
[34] H. T. Chifotides, K. R. Dunbar, *Acc. Chem. Res.* **2013**, *46*, 894–906.
[35] J.-Z. Liao, L. Meng, J.-H. Jia, D. Liang, X.-L. Chen, R.-M. Yu, X.-F. Kuang, C.-Z. Lu, *Chem. Eur. J.* **2018**, *24*, 10498–10502.
[36] B. L. Schottel, H. T. Chifotides, K. R. Dunbar, *Chem. Soc. Rev.* **2008**, *37*, 68–83.
[37] D.-X. Wang, Q.-Y. Zheng, Q.-Q. Wang, M.-X. Wang, *Angew. Chem. Int. Ed.* **2008**, *47*, 7485–7488; *Angew. Chem.* **2008**, *120*, 7595–7598.
[38] D. Tuo, W. Liu, X. Wang, X. Wang, Y. Ao, Q. Wang, Z. Li, D. Wang, *J. Am. Chem. Soc.* **2019**, *141*, 1118–1125.
[39] K. I. Assaf, W. M. Nau, *Angew. Chem. Int. Ed.* **2018**, *57*, 13968–13981; *Angew. Chem.* **2018**, *130*, 14164–14177.
[40] L. M. Skinner, J. R. Sambles, *J. Aerosol Sci.* **1972**, *3*, 199–210.
[41] M. Sadakane, E. Steckhan, *Chem. Rev.* **1998**, *98*, 219–237.
[42] I. V. Kozhevnikov, *Chem. Rev.* **1998**, *98*, 171–198.
[43] P. Gilli, V. Bertolasi, C. Ferretti, G. Gilli, *J. Am. Chem. Soc.* **1994**, *116*, 909–915.
[44] L. Nicolas, A. Magali, M. Nicolas, C. Elena, *Cryst. Growth Des.* **2011**, *11*, 5200–5205.
[45] Q. Han, L. Zhang, C. He, J. Niu, C. Duan, *Inorg. Chem.* **2012**, *51*, 5118–5127.